FORUM GEOGRAFI
ISSN: 0852-0682 | E-ISSN: 2460-3945

HTTPS://JOURNALS.UMS.AC.ID/INDEX.PHP/FG/

Validating the GIS-based Flood Susceptibility Model Using Synthetic Aperture Radar (SAR) Data in Sengah Temila Watershed, Landak Regency, Indonesia

Ajun Purwanto[1,*], Dony Andrasmoro[1], Eviliyanto Eviliyanto[1], Rustam Rustam[1], Mohd Hairy Ibrahim[2], Arif Rohman[3,4]

[1] Department of Geography Education, IKIP PGRI Pontianak, Jl. Ampera No.88, Sungai Jawi, Kec. Pontianak Kota, Kota Pontianak, Kalimantan Barat 78116, Indonesia
[2] Department Geography & Environment, Faculty Human Sciences, Universiti Pendidikan Sultan Idris, 35900 Tanjong Malim, Perak, Malaysia
[3] School of Geography, University of Leeds, Seminary St, Woodhouse, Leeds LS2 9JT, United Kingdom
[4] Geomatics Engineering, Institut Teknologi Sumatera, Jl. Terusan Ryacudu, Desa Way Hui, Kecamatan Jatiagung, Lampung Selatan 3536

[*)] Correspondance : ajunpurwanto@ikippgriptk.ac.id

Citation:
Purwanto, A., Andrasmoro, D., Eviliyanto, E., Rustam, R., Ibrahim, M.H., & Rohman, A. (2022) Validating the GIS-based Flood Susceptibility Model Using Synthetic Aperture Radar (SAR) Data in Sengah Temila Watershed, Landak Regency, Indonesia. Forum Geografi. Vol. 36, No. 2.

Article history:
Received: 22 November 2022
Accepted: 08 March 2023
Published: 30 March 2023

Abstract

In Indonesia, especially in regions where natural conditions and human activity coexist, flood disasters are a strong possibility. Flooding regularly has an impact on Sengah Temila, which is a component j/ of Indonesia's West Kalimantan Province. The issue in Sengah Temila is that there is little knowledge of the distribution of flood susceptibility in this region. The GIS-based flood susceptibility model has been widely used in Indonesia, but research dedicated to validating the model is limited. SAR-based analysis has been used for flood mapping in Indonesia, but its use for validating flood models has been limited. The objective of this study is to identify the optimal weighting scenario for a GIS-based multi-criteria analysis flood model for use in the Sengah Temila Watershed. The GIS-based model is created by merging spatial parameters, including slope, elevation, flow accumulation, drainage density, land use and land cover (LULC), soil type, normalized difference vegetation index (NDVI), curvature, rainfall, distance to river, and topographic wetness index (TWI) with weighted multi-criteria analysis. In addition, Sentinel-1 GRD images from before and after the floods have been retrieved from Google Earth Engine using past floods of the watershed. In order to create a SAR-based flood model, the researchers then integrated and categorized the results. Eleven weighting scenarios were used to create eleven GIS-based flood models. To calculate the degree of spatial similarity, all of these models were contrasted with the SAR-based model using the Fuzzy Kappa approach. We found that in order to achieve ideal weighting, slope, topographic wetness index (TWI), rainfall, and flow accumulation should each be given a larger value.

Keywords: Flood susceptibility, Watershed, GIS, Synthetic Aperture Radar, and Landak Regency.

1. Introduction

Floods are a frequent occurrence in Indonesia, impacting various regions of the country. This natural disaster is a logical phenomenon, given Indonesia's tropical location and high rainfall levels. Floods can be deadly regardless of whether a country is developed or developing. Both types of countries can be affected by the devastating consequences of floods (Petrucci, 2022). As a result, it is crucial for all countries to prioritize flood prevention and mitigation efforts to minimize the damage caused by these disasters. By implementing effective measures, such as building robust infrastructure and enhancing disaster preparedness, countries can reduce the loss of life and property caused by floods (Rohman *et al*., 2019). Despite the challenges posed by these disasters, taking proactive steps to address them can help ensure the safety and well-being of people in flood-prone areas. These natural disasters have significant effects on human life. Floods are one of the most pervasive natural hazards impacting populations, and they have negative effects upon many aspects of society, such as social structures (including loss of human life and adverse physical and mental health effects on the population) (Geographic, 2019; Rincón *et al*., 2018), infrastructure and essential services, crops and livestock animals, and public health (the spread of diseases) and the contamination of water supplies (Rincón *et al*., 2018).Increasingly, floods occur due to effects of climate change, such as higher levels of rainfall, which cause river beds to rise. Flood occurrence has increased significantly worldwide in the last three decades (Komolafe *et al*., 2020; Rozalis *et al*., 2010).

Several factors cause the floods. Land structure, vegetation, and inclination are all features of flood-prone areas, yet humans themselves are also directly causing floods, in addition to human-created climate-change (Curebal *et al*., 2016). Another essential factor is land-use changes, such as deforestation and urbanization (Rincón *et al*., 2018). Floods also result from complex hydrological, geological, and geomorphological conditions, deforestation, and urbanization, and produce substantial social, economic, and environmental damage (Falguni & Singh, 2020; Komolafe *et al*., 2020; Skilodimou *et al*., 2019). Floods are evident in the loss of human life and other

negative effects on populations, infrastructural damage, damage to crops and livestock and wild animals, and even the loss of entire ecosystems. The spread of diseases and water supply contamination may also result from flooding (Rincón *et al*., 2018).

Floods are the most dynamic natural disaster. They cannot be simply partially prevented, but must be comprehensively prevented. With good risk assessments, the occurrence of a flood can be forecasted, and flood damage can be mitigated. In recent years, a growing number of studies on flood risk assessment and analysis has been undertaken in different regions and cities both in the lowlands end coastal areas of Indonesia (Cai *et al*., 2021; Sarmah *et al*., 2020), comparatively little investigation has been performed on upstream areas which are mountainous regions. Areas in mountain cities are sensitive to sudden floods on account of large elevation disparities and other specific factors (Romanescu *et al*., 2018).

West Kalimantan, especially Sengah Temila Watershed, has had many experiences of flood disasters. For instance, In January 2021, heavy rainfall in the West Kalimantan region caused significant flooding in several sub-districts, including Sengah Temila District in Landak Regency. The impact of the flood was severe, and the flood caused water to rise in several villages up to the road and into the houses of residents. The water level varied, and some areas in the district also even experienced landslides. This was not the first time Sengah Temila District had faced such flooding; residents had previously been forced to evacuate when the water level reached a height of 3.5 to 4 meters. The area is prone to flooding, and it is important to understand the flood distribution and potential solutions to mitigate the impact on the local population (Post, 2021). Therefore, developing a flood hazard model to identify areas susceptible to flooding is essential for decision-makers to undertake comprehensive flood risk management (Allafta & Opp, 2021). Such information is essential for early warning systems, emergency services, the prevention and mitigation of future floods, and the implementation of flood management strategies (Krzysztofowicz, 1993; Bubeck *et al*., 2012; Falguni & Singh, 2020; Mandal & Chakrabarty, 2016; Shafapour Tehrany *et al*., 2017).

Various techniques have also been developed to monitor flood disasters, including Remote Sensing and Geographic Information Systems. Remote Sensing has made a substantial contribution to flood monitoring and damage assessment, enabling the disaster management authorities to contribute significantly to plans to prevent the impact of future floods (Haq *et al*., 2012). The Geographical Information System (GIS) has also made a significant contribution in this area (Vojtek, 2019). In addition, various techniques for mapping flood vulnerability and extent, and for assessing flood damage have been developed. The goal of these efforts is to provide a guide for the operation of Remote Sensing (RS) and Geographic Information Systems (GIS) to improve the efficiency of monitoring and managing flood disasters (Haq *et al*., 2012).

Recent studies have also demonstrated the use of GIS and remote sensing technologies to map the spatial variability of flooding events and flood hazards (Elkhrachy, 2015; Greene & Cruise, 1995; Islam & Sado, 2000; Ozkan & Tarhan, 2016; Paudyal, 1996; Shafapour Tehrany *et al*., 2017). This research has adopted a multi-layered approach for flood mapping to improve the accuracy of coarse grid modelling with only a minor increase to the computing cost (Chen *et al*., 2012; Zhou *et al*., 2021). This work has included the development of the Cellular Automata (CA) approach using regular grid cells and generic rules to simulate the spatiotemporal evolution of pluvial flooding, which significantly reduced computation time (Ghimire *et al*., 2013) and developing an Urban Storm Inundation Simulation Method (USISM) using GIS-based simplified distributed hydrological models with DEM inputs (Zhang & Pan, 2014). Jamali *et al*. developed an urban pluvial flood model by integrating a 1D hydraulic drainage network model and GIS technology to rapidly estimate flood extent, depth, and associated damage (Jamali *et al*., 2018).

Geographical Information Systems (GIS) and Remote Sensing (RS) can provide tremendous potential for flood identification, monitoring, and assessment (Biswajeet & Mardiana, 2009; Haq *et al*., 2012; Pradhan *et al*., 2009). GIS can be used to produce a susceptibility map based on the overlay of influencing flood factors (Negese *et al*., 2022). On the other hand, remote sensing data such as Synthetic Aperture Radar (SAR) can be used to monitor ground change after flood events. By applying change detection to the data for flood-affected areas, researchers can map flood impact (Anusha & Bharathi, 2020; Clement *et al*., 2018; Li *et al*., 2018; Mason *et al*., 2014; Tay *et al*., 2020). Therefore, GIS-based and SAR-based flood models can be compared to determine the optimum weighting scenario. The objective of this study is to identify the optimal weighting scenario for a GIS-based multi-criteria analysis flood model in the Sengah Temila Watershed.

2. Research Method

2.1. Study Area

The research was undertaken in the Sengah Temila District, Landak Regency, West Borneo Province, Indonesia, located between longitude 109°34'30"E to 109°47'30"E and latitude 0°14'30"N to 0°27'30"N (Figure 1). The study area is approximately 53.677,81 ha (536,7781 km^2). The Sengah Temila Watershed covers eleven villages, including Senakin, Gombang, Baying, Sidas, Keranji Mancal, Paloah, Pahuman, Saham, Keranji Padang, Sebatih, and Kampung Tengah.

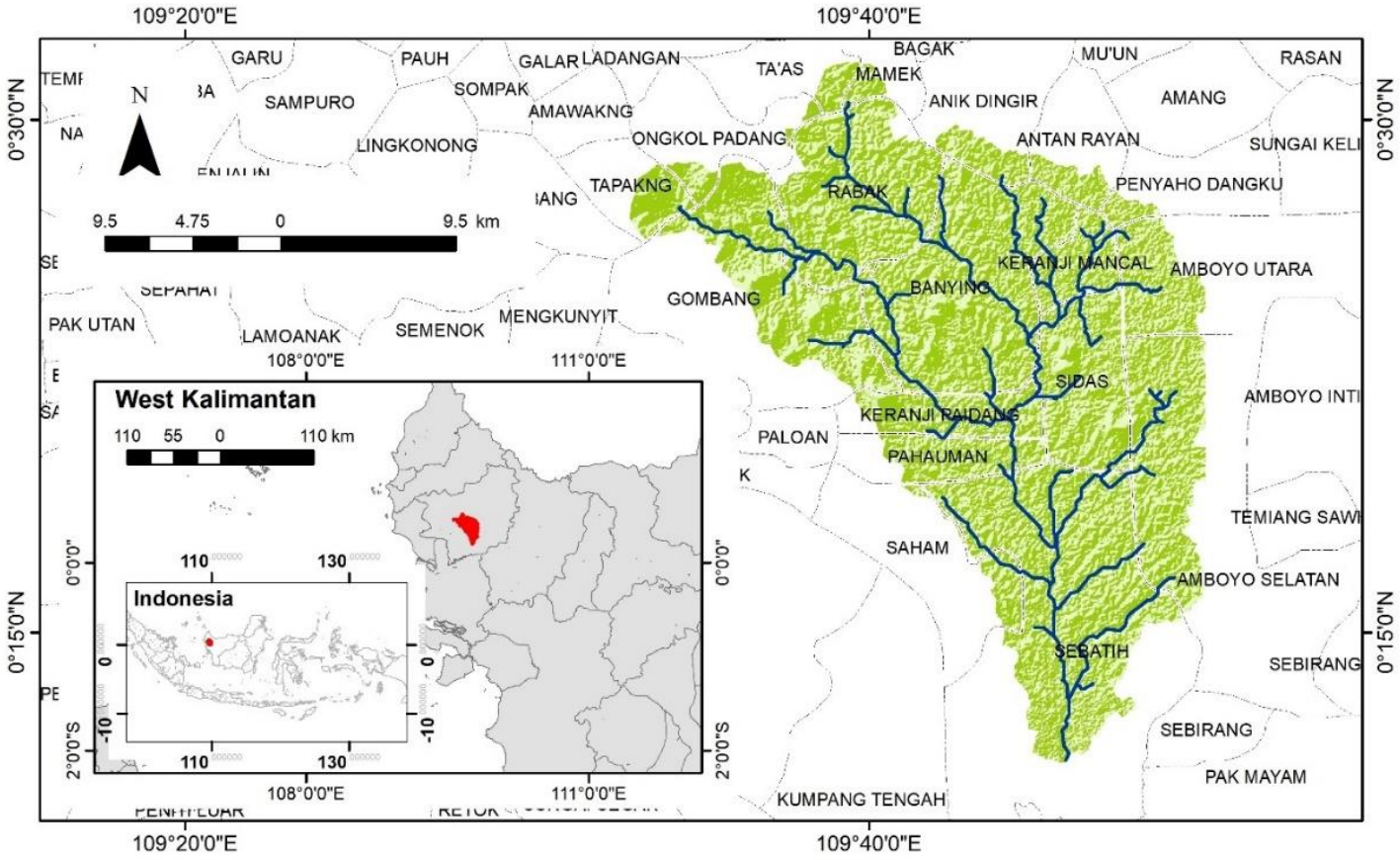

Figure 1. Study Area.

2.2. Research Framework

In this study, a GIS-based flood model was created by merging spatial parameters with weighted multi-criteria analysis and validated with Synthetic Aperture Radar (SAR)-based flood susceptibility data (Figure 2). The flood susceptibility maps in the study area were created by combining various factors (Section 2.4). Eleven weighting scenarios were used to create eleven GIS-based flood models by means of weighted overlay (Section 2.5). To create the SAR-based flood model, we retrieved Sentinel-1 GRD images recorded in the watershed before and after past flood events from Google Earth Engine (Section 2.6). The results from the GIS-based models and the SAR-based model were integrated and categorized. GIS-based maps of all scenarios were then contrasted with a SAR-based flood model. The fuzzy Kappa approach was used to calculate the degree of spatial similarity (Section 2.7).

2.3. Data Collection

To carry out the flood susceptibility study, the researchers drew on various data sources (Table 1). These sources included the SRTM-DEM from USGS used for the Digital Elevation Model (DEM) data. The soil type data was obtained from the West Kalimantan Soil Type Map, while the rainfall data was obtained from the West Kalimantan rainfall measurement stations. The Sentinel-2 MSI image and Sentinel-1 GRD image were both obtained from Google Earth Engine to provide data on land cover and land use as well as vegetation cover. These data sources were essential in the production of the flood susceptibility maps, which were produced through the development of weighted overlays of the various flood factors in ArcGIS. The combination of

these data sources and the GIS and remote sensing techniques used enabled the creation of comprehensive flood susceptibility maps for the study area.

Table 1. Data Sources.

No	Flood Parameters	Data Source
1	DEM	SRTM-DEM from USGS
2	Soil Type	West Kalimantan Soil Type Map
3	Rainfall data	West Kalimantan rainfall measurement stations
4	Sentinel-2 MSI Image	Google Earth Engine
5	Sentinel-1 GRD Image	Google Earth Engine

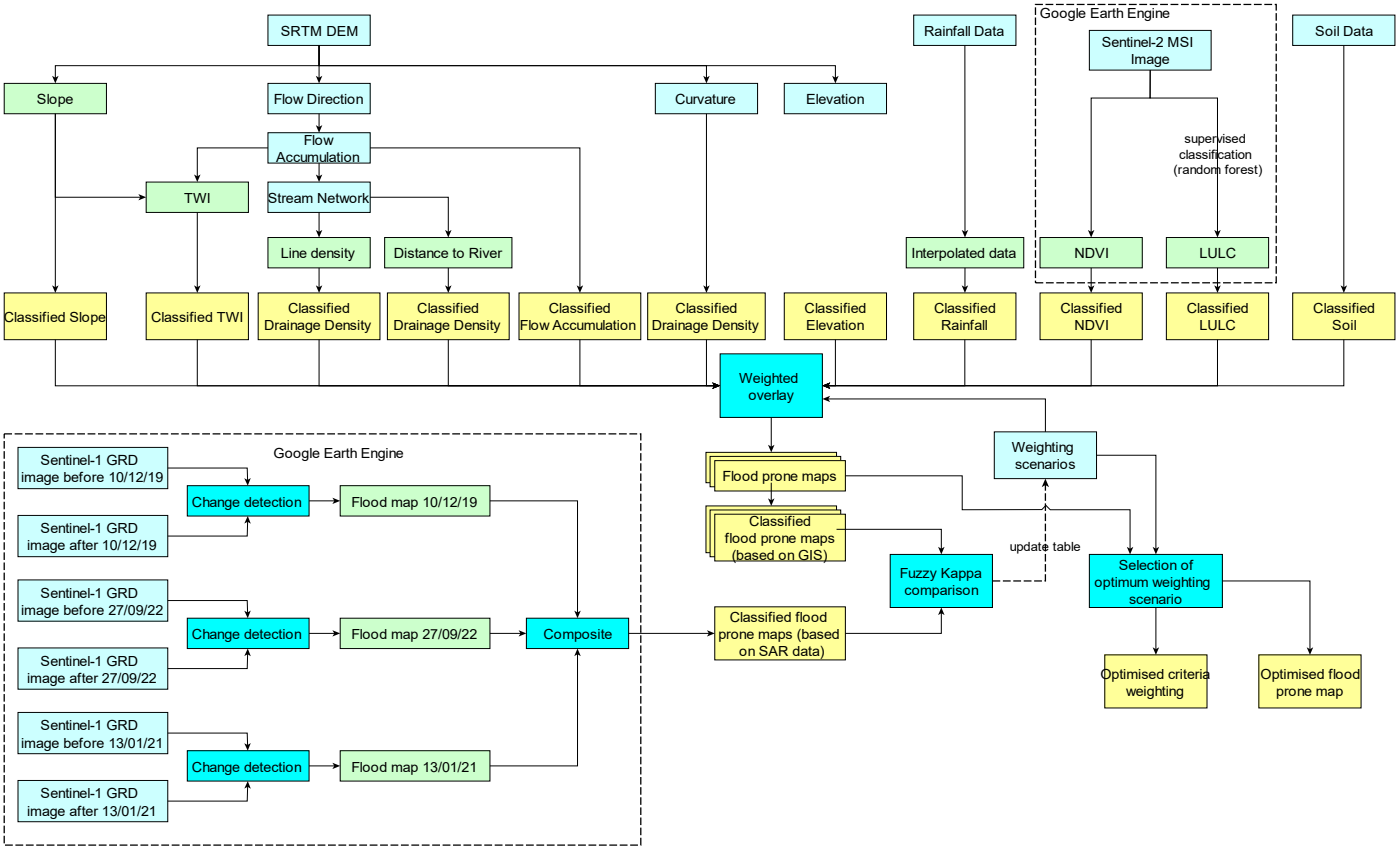

Figure 2. Research Framework.

2.4. Flood Susceptibility Factors

Flood susceptibility is determined by evaluating a range of factors that include slope, elevation, flow accumulation, drainage density, land use and land cover (LULC), soil type, normalized difference vegetation index (NDVI), curvature, rainfall, distance to river, and topographic wetness index (TWI). The speed of surface water flow is governed by the slope of the terrain, with lowlands or flatlands having a higher likelihood of flood inundation due to the increase in water accumulation and decrease in water flow speed. Elevation and distance to the river are significant determinants, with lower elevated locations and areas closer to rivers having a higher probability of flooding due to their relatively higher river discharge and slower water flow. Flow accumulation and drainage density influence the likelihood of flood occurrence, with higher flow build-up and drainage density increasing the probability of flooding. LULC plays a vital role in determining flood susceptibility, with areas with a high density of vegetation being less susceptible to flood risk due to the slower flow of water and higher infiltration. Soil type is also a crucial factor, with fine soil texture enhancing surface runoff and decreasing infiltration, increasing the probability of flooding. NDVI and curvature are additional parameters that contribute to flood susceptibility,

with increased vegetation density slowing down runoff, and areas with flat curvature being the most vulnerable to flooding. Finally, rainfall and TWI are key determinants, with heavy precipitation increasing water accumulation and TWI indicating locations with potentially saturated land surfaces, both resulting in a higher probability of flood inundation.

2.5. GIS-based Flood Maps Preparation

The weighted overlays produced using ArcGIS were used to combine all flood components and create the GIS-based flood susceptibility maps. Elevation (El), slope of the land (Sl), flow accumulation (FA), distance to rivers (DR), rainfall (Rf), drainage density (DD), topographic wetness index (TWI), land use land cover (LULC), Normalized Difference Vegetation Index (NDVI), soil type (ST), and curvature of the land surface (Cu) are the eleven factors that affect the occurrence of floods. Spatial data layers of these eleven factors were prepared in a raster format.

The West Kalimantan Soil Type Map was extracted using ArcGIS 10.8 software to identify the soil types of the watershed, and the recovered vector soil map was then transformed into a raster format. Areas of the district's digital elevation model (DEM) map were classed into five groups based on susceptibility to flooding. Using the slope and curvature tools in the Spatial Analyst Tools of the ArcGIS environment, researchers produced the slope and curvature maps directly from the DEM map of the study area.

The district's DEM map was filled in to create a sink-free/depression-free DEM, and the flow direction map was then created using the filled-in DEM map. The flow direction map was then used to construct the flow accumulation raster map. Hydrology capabilities calculated using the Spatial Analyst Tools of ArcGIS software, such as Fill, Flow Direction, and Flow Accumulation, were used to fill the DEM map, create flow direction, and calculate flow accumulation. By using the supervised classification with a random forest algorithm on a Sentinel 2 MSI image from a 2019 acquisition, the researchers produced LULC drawing on information from Google Earth Engine.

The yearly average precipitation data from the West Kalimantan rainfall measurement station were imported into ArcGIS software to construct the rainfall point data of meteorology stations. In order to create a continuous rainfall map of the district, the researchers then interpolated the mean yearly rainfall of the five sites using the Inverse Distance Weighted (IDW) method in ArcGIS 10.8.

Using the Raster Calculator tool in the ArcGIS environment, the researchers produced the drainage network map from the flow accumulation map, and afterwards, the drainage density map was produced from the drainage network map using the Line Density tool included in the Spatial Analyst Tools of ArcGIS 10.8 program. After the rivers in the research area were extracted from the river network data, the Euclidean Distance tool found in the Spatial Analyst Tools of ArcGIS environment was used to construct a distance to the river raster map.

The Moore *et al*. (1991) equation (Equation 1) was used to create the Topographic Wetness Index (TWI) map of the watershed.

$$\mathrm{TWI} = \mathrm{Ln}\left(\frac{A_s}{\tan B}\right) \qquad (1)$$

where TWI represents the topographic wetness index, A s rep resents the cumulative upslope area draining through a point (per unit contour length), and B represents the local slope angle in degrees. The TWI map was created using the Raster Calculator available in the Spatial Analyst Tools in the ArcGIS environment. The district's NDVI map was created using Google Earth Engine and a Sentinel 2 MSI satellite image. The Normalized Difference Vegetation Index, or NDVI, was calculated by using equation (Equation 2):

$$\mathrm{NDVI} = \frac{(NIR - RED)}{(NIR + RED)} = \frac{(Band\ 8 - Band\ 4)}{(Band\ 8 + Band\ 4)} \qquad (2)$$

where NIR stands for surface spectral reflectance in the near-infrared band (band 8 in the Sentinel 2 MSI picture), and RED is for surface spectral reflectance in the red band (which is band 4 in the Sentinel 2 MSI image).

Table 2. Flood Susceptibility Factors.

No	Factor	Classification	Susceptibility	Score
1	Slope (Sl) (Degree)	> 45	Very Low	1
		25-45	Low	2
		15-25	Moderate	3
		8-15	High	4
		0-8	Very High	5
2	Rainfall (Rf) (mm)	1,696-1,728	Very Low	1
		1,728-1,761	Low	2
		1,761-1,793	Moderate	3
		1,793-1,825	High	4
		> 1,825	Very High	5
3	Drainage Density (DD) (km/km^2)	0-0.372	Very Low	1
		0.372-0.754	Low	2
		0.754-1.106	Moderate	3
		1.106-1.519	High	4
		>1.519	Very High	5
4	Soil Type (ST)	Ultisol	Very Low	2
		Inseptisol	Low	3
		Histosol	Moderate	4
		Oxisol	Very High	5
5	Land Use/ Land Cover (LULC)	Dense Vegetation	Very Low	1
		Bareland	Low	2
		Open Mining	Moderate	3
		Cropland	High	4
		Built-up area	Very High	5
6	Elevation (El) (m amsl)	558.8 - 697	Very Low	1
		420.6 - 558.8	Low	2
		282.4 - 420.6	Moderate	3
		144.2 - 282.4	High	4
		6 - 144.2	Very High	5
7	Distance to river (DR) (m)	0.372 - 1.2976	Very Low	1
		1.2976 - 2.2232	Low	2
		2.2232 - 3.1488	Moderate	3
		3.1488 - 4.0744	High	4
		4.0744 - 5	Very High	5
8	NDVI	– 0.16–0.29	Very Low	1
		0.29–0.38	Low	2
		0.38–0.45	Moderate	3
		0.45–0.51	High	4
		0.51–0.59	Very High	5
9	Curvature (Ct)	Convex (positive)	Moderate	1
		Concave (negative)	High	2
		Flat	Very High	3
10	Flow Accumulation (FA)	< 250	Very Low	1
		250–2195	Low	2
		2195–3415	Moderate	3
		3415–15,125	High	4
		< 250	Very High	5
11	Topographic Wetness Index (TWI)		Very Low	1
		2.48–5.91		
		5.91–8.09	Low	2
		8.09–10.18	Moderate	3
		10.18–12.63	High	4
		12.63–22.77	Very High	5

The flood-controlling parameters were first prepared in raster format, and then they were rescaled to the same geographic resolution and classed into five common measurement scales, ranging from 1 (extremely low susceptibility to flooding) to 5 (very high susceptibility to flooding) (Table 2). Areas more sensitive to flooding have a higher classed ranking value of (5), while those less

susceptible to flooding have a lower value (1). Eleven weighting scenarios were employed using a GIS-based technique to produce different flood models (Table 3). Such weighting scenarios establish the relative value of several flooding-related factors. With a variety of potential outcomes, each scenario represents a unique mix of weightings given to the components. The GIS analysis was automated using Python script (Appendix 1) to perform all scenarios.

Table 3. Scenarios of Weighting.

	Weight of Factor											Total
Scenario	Sl	Rf	DD	ST	LULC	El	DR	NDVI	Ct	FA	TWI	
1	0.0051	0.0026	0.0013	0.0005	0.0003	0.5144	0.2572	0.1286	0.0514	0.0257	0.0129	1
2	0.1538	0.0769	0.0308	0.0154	0.0077	0.0077	0.0154	0.0769	0.1538	0.3077	0.1538	1
3	0.0833	0.0333	0.0167	0.0083	0.0083	0.0167	0.0833	0.1667	0.3333	0.1667	0.0833	1
4	0.0351	0.0175	0.0088	0.0088	0.0175	0.0877	0.1754	0.3509	0.1754	0.0877	0.0351	1
5	0.0179	0.0089	0.0089	0.0179	0.0893	0.1786	0.3571	0.1786	0.0893	0.0357	0.0179	1
6	0.009	0.009	0.018	0.0901	0.1802	0.3604	0.1802	0.0901	0.036	0.018	0.009	1
7	0.009	0.018	0.0901	0.1802	0.3604	0.1802	0.0901	0.036	0.018	0.009	0.009	1
8	0.0179	0.0893	0.1786	0.3571	0.1786	0.0893	0.0357	0.0179	0.0089	0.0089	0.0179	1
9	0.0833	0.1667	0.3333	0.1667	0.0833	0.0333	0.0167	0.0083	0.0083	0.0167	0.0833	1
10	0.1538	0.3077	0.1538	0.0769	0.0308	0.0154	0.0077	0.0077	0.0154	0.0769	0.1538	1
11	0.2667	0.1333	0.0667	0.0267	0.0133	0.0067	0.0067	0.0133	0.0667	0.1333	0.2667	1

2.6. SAR-based Flood Maps Preparation

By using Sentinel-1 Synthetic Aperture Radar (SAR) data in Google Earth Engine (GEE), a researcher can use flood mapping and damage assessment as a technique utilizing remote sensing data to detect and quantify flood events in a particular area. Sentinel-1 SAR data is very helpful for this because it can lead to the creation of imagery of flood events even in places with constant cloud cover because it can see through clouds and rain. The mapping of floods and damage assessment utilizing Sentinel-1 GRD data in GEE involves several steps. The area of interest's Sentinel-1 SAR data is first collected. SAR image captured at various times are then compared to identify changes in the landscape brought on by flooding (change detection). Using this method, the researcher can produce flood extent maps that display the areas that have been flooded. This study compares three pairs of Sentinel-1 GRD for three flood events (Figure 3) in GEE using UN SPIDER (2019) script. After the data were compared, the results were downloaded and clipped into the study area and combined to create a composite image using ArcGIS 10.8. To create a SAR-based flood model, the researchers reclassified the composite image into three categories based on the pixel value.

2.7. Comparison Analysis and Weighting Selection

To determine the ideal weighting scenario, raster datasets from flood maps created using GIS and SAR were compared spatially. The degree to which the output of the simulation and the actual data were similar was assessed using fuzzy Kappa (K*) without a smoothing function (Hagen-Zanker, 2006; Robinson & Rai, 2015). Map The Comparison Kit 3.2 software developed by Visser and Nijs (Visser & Nijs, 2006) was used to perform this analysis. Fuzzy kappa is a statistical tool for evaluating the degree of agreement between two sets of ratings or classifications. It is frequently utilised in disciplines like remote sensing, ecology, and image processing where there is frequently uncertainty when classifying or categorising objects. The standard kappa coefficient, which gauges the degree of agreement between two sets of categorical data, has been modified to create fuzzy kappa. Instead of treating membership as an all-or-nothing notion, Fuzzy Kappa considers the degree of membership of each item in each class.

Figure 3. Flood Events in Sengah Temila. (a) 10 December 2019, (b) 13 January 2021, (c) 27 September 2022.

3. Results and Discussion

3.1. Flood Parameters

Figure 4 presents an overview of variables of the study area, including elevation, curvature, distance to river, drainage density, flow accumulation, land use/land cover (LULC), normalized difference vegetation index (NDVI), rainfall, slope, soil, and topographic wetness index (TWI). The percentage values represent the proportion of the region falling within a given range for each factor. The majority of the region lies between 558.8 and 697 meters above sea level, with convex and concave curvature equally distributed and only a small amount of flat surface. The distance from rivers varies, with the majority of the region located between 4.0744 and 5 meters from a river. Drainage density ranges from 2.48 to 5.91 meters per kilometer, indicating a well-established drainage network. Flow accumulation is often low, and NDVI is low in most of the area. The region receives modest amounts of precipitation, with the majority receiving between 1,761 and 1,793 millimeters annually; that is, based on this parameter, it falls within the category of moderate flood susceptibility (Adiat *et al*., 2012; Blistanova *et al*., 2016; Gazi *et al*., 2019; Hagos *et al*., 2022). Slope ranges from 41.28 to 51.6 degrees, making the area prone to flood (Desalegn & Mulu, 2021; Gigović *et al*., 2017; Hagos *et al*., 2022; Rimba *et al*., 2017; Singh *et al*., 2020; Wondim, 2016). Most of the land is categorized as histosol, indicating a potential for agriculture. TWI values between 5.91 and 8.09 suggest a generally well-drained watershed.

The factors that determine an area's susceptibility to flooding, such as elevation, curvature, distance to river, drainage density, flow accumulation, land use and land cover, normalized difference vegetation index (NDVI), rainfall, slope, soil, and topographic wetness index (TWI) were then reclassified to describe the area's level of susceptibility to flooding (Figure 5). The susceptibility to flooding ranges from very low to very high, depending on each factor (Table 4). For instance, elevation has a susceptibility that ranges from very low to very high, with the most susceptible areas having a very low elevation; these account for 58.78% of the area. Curvature, which describes the shape of the land surface, has a susceptibility that ranges from moderate to very high, with the most susceptible areas having a high curvature; they account for 42.27% of the total land area. Land use and land cover (LULC) and NDVI, which describe the way the land is used and the density of vegetation, respectively, also have varying degrees of susceptibility. The most susceptible areas for LULC have high coverage and account for 32.82% of the area, while the least susceptible areas have a very low LULC and account for 64.99% of the area. The most susceptible areas for NDVI have a very low NDVI and account for 92.24% of the area, while the least susceptible areas have a very high NDVI and account for only 0.001% of the area. Other factors, such as rainfall, slope, and distance to river, also have varying degrees of susceptibility that range from very low to very high.

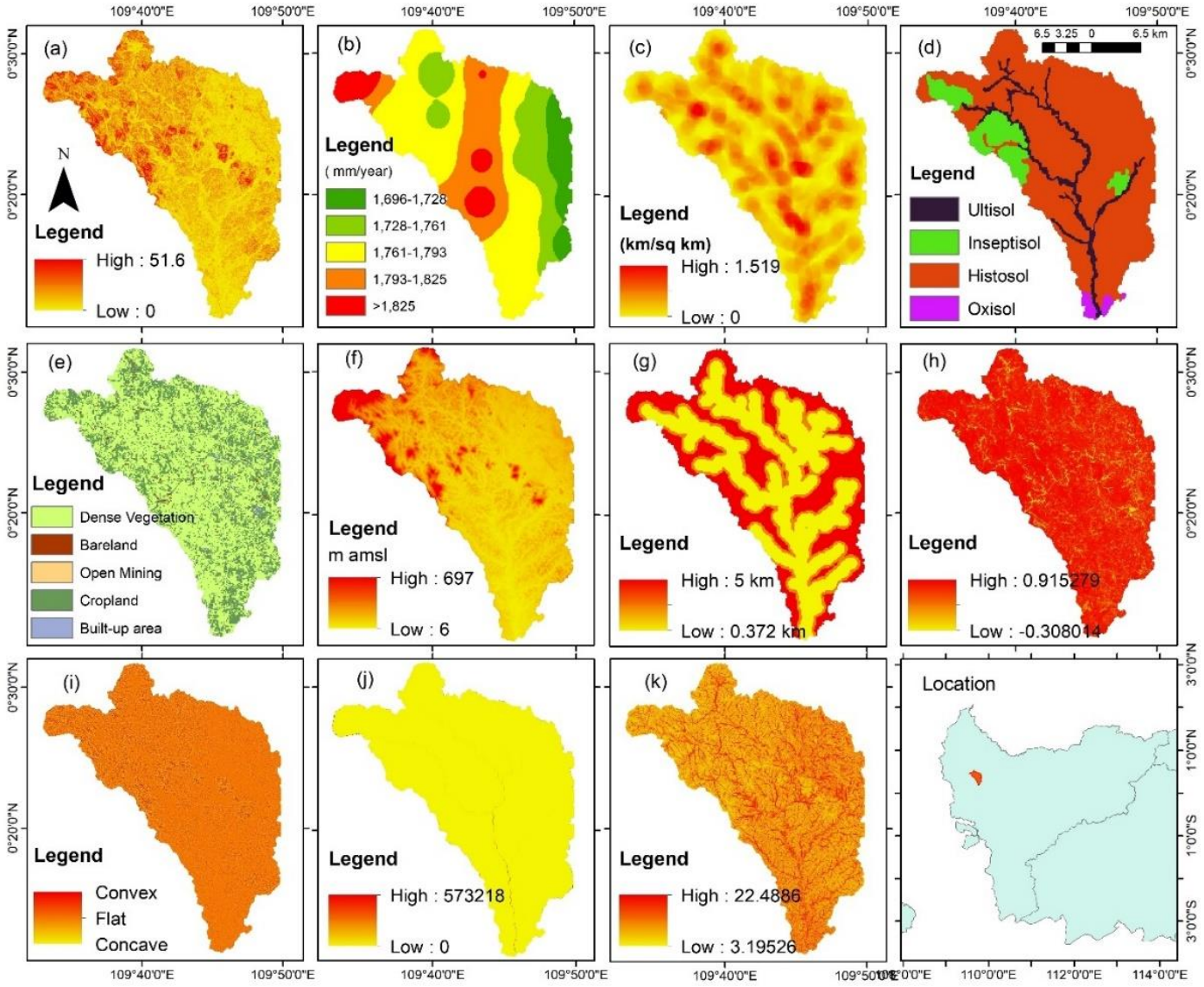

Figure 4. Spatial Parameters of Flood Prone Land Analysis, where from (a) to (k), respectively: Slope (Sl)(Degree), Rainfall (Rf) (mm), Drainge Density (DD) (km/km2), Soil Type (ST), Use/ Land Cover (LULC), Elevation (El) (m amsl), Distance to river (DR) (m), Normalized Difference Vegetation Index (NDVI), Curvature, Flow Accumulation (FA), Topographic Wetness Index (TWI).

Table 4. Coverage of Susceptibility Parameters.

No	Factor	Susceptibility	Classification	Area (km^2)	Percentage (%)
1	Slope (Sl) (Degree)	1	0 - 10.32	20.17536891	4
		2	10.32 - 20.64	57.74509658	10
		3	20.64 - 30.96	105.7560777	19
		4	30.96 - 41.28	161.3533166	29
		5	41.28 - 51.6	211.8123019	38
2	Rainfall (Rf) (mm)	1	1,696-1,728	47.6062166	8.549
		2	1,728-1,761	103.4974789	18.587
		3	1,761-1,793	245.5360251	44.094
		4	1,793-1,825	120.4584208	21.632
		5	> 1,825	39.80428579	7.148

Table 4. Continued.

No	Factor	Susceptibility	Classification	Area (km^2)	Percentage (%)
3	Drainage Density (DD) (km/km2)	1	0-0.372	335.1219083	60
		2	0.372-0.754	159.8936527	29
		3	0.754-1.106	48.22260636	9
		4	1.106-1.519	11.11493465	2
		5	>1.519	2.914672738	1
4	Soil Type (ST)	2	Ultisol	45.93877282	8.2
		3	Inseptisol	57.16224052	10.3
		4	Histosol	445.7271287	80.0
		5	Oxisol	8.439632687	1.5
5	Land Use/ Land Cover (LULC)	1	Dense Vegetation	361.9016776	65.0
		2	Bareland	4.391101662	0.8
		3	Open Mining	0.586433727	0.1
		4	Cropland	182.7386911	32.8
		5	Built-up area	7.065828148	1.269
6	Elevation (El) (m amsl)	1	558.8 - 697	327.2914272	59
		2	420.6 - 558.8	160.9820238	29
		3	282.4 - 420.6	43.64639013	8
		4	144.2 - 282.4	17.78280602	3
		5	6 - 144.2	7.139514457	1
7	Distance to river (DR) (m)	1	0.372 - 1.2976	109.2347316	20
		2	1.2976 - 2.2232	86.93984274	16
		3	2.2232 - 3.1488	97.16299504	17
		4	3.1488 - 4.0744	122.8947972	22
		5	4.0744 - 5	140.6438858	25
8	NDVI	1	– 0.16–0.29	513.6085072	92.236
		2	0.29–0.38	40.82692437	7.332
		3	0.38–0.45	2.360937851	0.424
		4	0.45–0.51	0.123366084	0.022
		5	0.51–0.59	0.007151589	0.001
9	Curvature (Ct)	3	Convex (positive)	209.9995875	38
		4	Concave (negative)	235.4017622	42
		5	Flat	111.4409723	20
10	Flow Accumulation (FA)	1	< 250	556.0045996	99.85
		2	250–2195	0.268791525	0.05
		4	2195–3415	0.23080077	0.04
		5	3415–15,125	0.338130133	0.06
		1	2.48–5.91	182.741257	32.8
11	Topographic Wetness Index (TWI)	2	5.91–8.09	242.5473129	43.6
		3	8.09–10.18	81.83121724	14.7
		4	10.18–12.63	34.51352499	6.2
		5	12.63–22.77	15.20900991	2.7

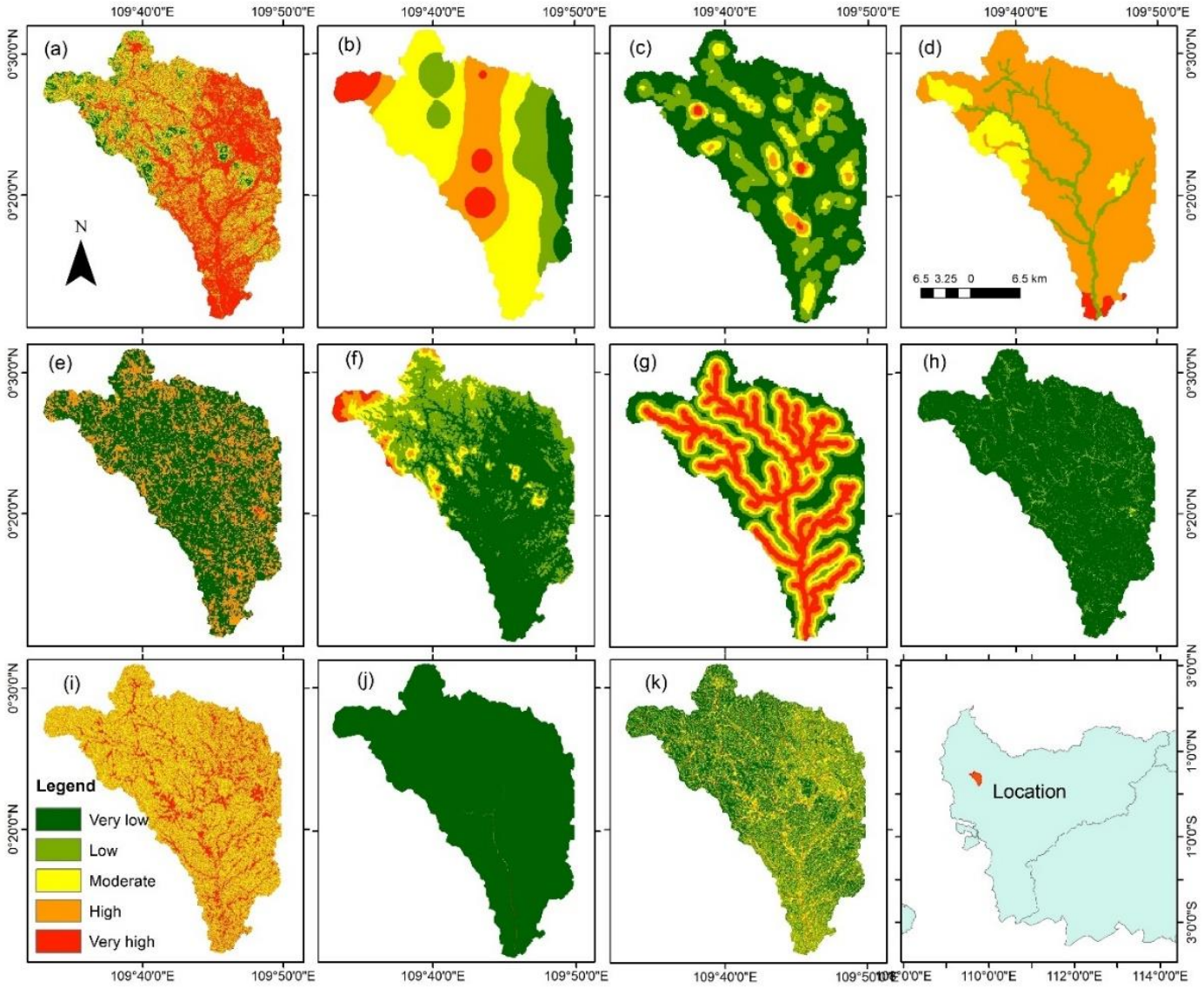

Figure 5. Reclassification of Spatial Parameters of Flood Prone Analysis, where from (a) to (k), respectively: Slope (Sl), Rainfall (Rf), Drainage Density (DD), Soil Type, Use/ Land Cover (LULC), Elevation (El), Distance to river (DR), Normalized Difference Vegetation Index (NDVI), Curvature, Flow Accumulation (FA), Topographic Wetness Index (TWI).

3.2. The Optimum Weighting Scenario

Based on the data provided for the scenario of weighting factors for GIS-based flood susceptibility (Table 5), it is clear that certain factors play a more important role than others. The most ideal scenario compared to the SAR-based flood susceptibility model (Figure 6), scenario 11, shows that the weighting of slope, topographic wetness index (TWI), rainfall, and flow accumulation should each be given a larger value; these factors are the most significant in determining flood susceptibility (Figure 7). Slope, which quantifies the steepness of the land surface, is a critical factor in determining flood susceptibility. The steeper the slope, the more water runoff will occur, which can lead to flooding. Similarly, the topographic wetness index (TWI) takes into account the ability of the land to retain water, with higher values indicating greater water retention capacity. This factor can also significantly impact the occurrence of floods. Rainfall and flow accumulation are also crucial factors in determining flood susceptibility. High levels of rainfall can result in increased water runoff. Flow accumulation, on the other hand, measures the volume of water that accumulates in a particular area. Higher flow accumulation values may indicate the potential for flooding, as there is a greater volume of water that maybe released during heavy rainfall. Therefore, the results suggest that these factors should be given more weight in GIS-based flood

susceptibility models. By doing so, researchers can make more accurate predictions about the areas that are most susceptible to flooding.

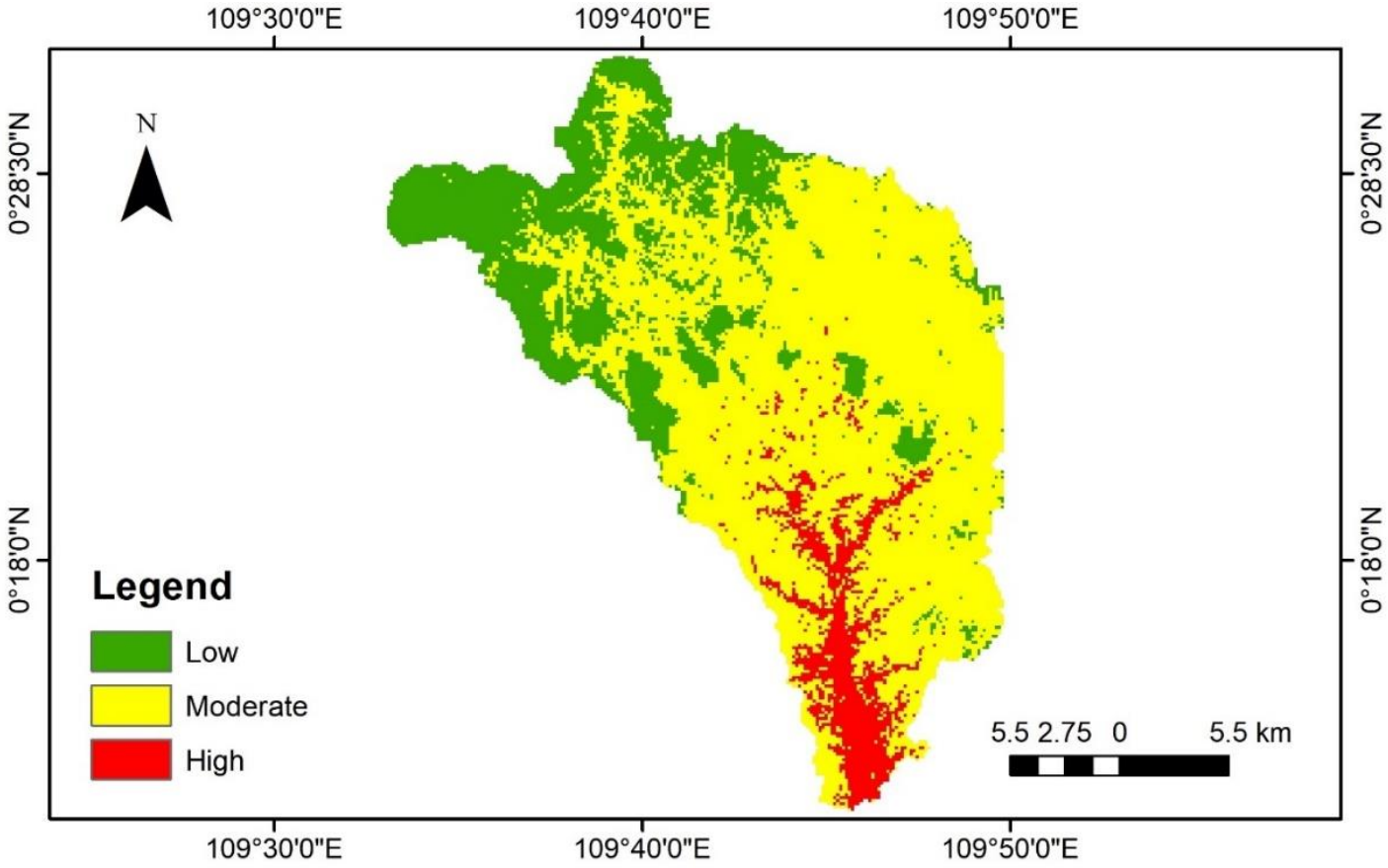

Figure 6. SAR-based Flood Susceptibility Map.

Table 5. Comparison Results of the Scenarios.

	Weight of Factor											K*
Scenario	Sl	Rf	DD	ST	LULC	El	DR	NDVI	Ct	FA	TWI	
1	0.0051	0.0026	0.0013	0.0005	0.0003	0.5144	0.2572	0.1286	0.0514	0.0257	0.0129	0.32
2	0.1538	0.0769	0.0308	0.0154	0.0077	0.0077	0.0154	0.0769	0.1538	0.3077	0.1538	0.68
3	0.0833	0.0333	0.0167	0.0083	0.0083	0.0167	0.0833	0.1667	0.3333	0.1667	0.0833	0.76
4	0.0351	0.0175	0.0088	0.0088	0.0175	0.0877	0.1754	0.3509	0.1754	0.0877	0.0351	0.55
5	0.0179	0.0089	0.0089	0.0179	0.0893	0.1786	0.3571	0.1786	0.0893	0.0357	0.0179	0.60
6	0.009	0.009	0.018	0.0901	0.1802	0.3604	0.1802	0.0901	0.036	0.018	0.009	0.44
7	0.009	0.018	0.0901	0.1802	0.3604	0.1802	0.0901	0.036	0.018	0.009	0.009	0.53
8	0.0179	0.0893	0.1786	0.3571	0.1786	0.0893	0.0357	0.0179	0.0089	0.0089	0.0179	0.68
9	0.0833	0.1667	0.3333	0.1667	0.0833	0.0333	0.0167	0.0083	0.0083	0.0167	0.0833	0.67
10	0.1538	0.3077	0.1538	0.0769	0.0308	0.0154	0.0077	0.0077	0.0154	0.0769	0.1538	0.72
11	0.2667	0.1333	0.0667	0.0267	0.0133	0.0067	0.0067	0.0133	0.0667	0.1333	0.2667	0.80

3.2. Discussion

According to the study, in order to achieve the best weighting scenario, slope, topographic wetness index (TWI), rainfall, and flow accumulation should each be assigned a higher value. The steepness of the terrain is referred to as the slope, and it can affect the volume and pace of water flow

during a rainstorm event. The topographic wetness index (TWI), which assesses the likelihood of saturation, is a useful tool for identifying possible floodplains. Rainfall is an important component in flood modelling because it is the main cause of flood disasters. Flood danger can also be significantly influenced by flow accumulation, which is a measurement of the volume of water flowing into a certain location. Slope has been used as a dominant factor in other studies (Alemayehu, 2007; Wondim, 2016). This variable indicates the velocity of water flowing through drainage channels and watersheds (Hagos *et al*., 2022). On the other hand, the possibility for overland flow can be predicted by the Topographic Wetness Index, which can help researchers identify locations with potentially saturated land surfaces (Negese *et al*., 2022).

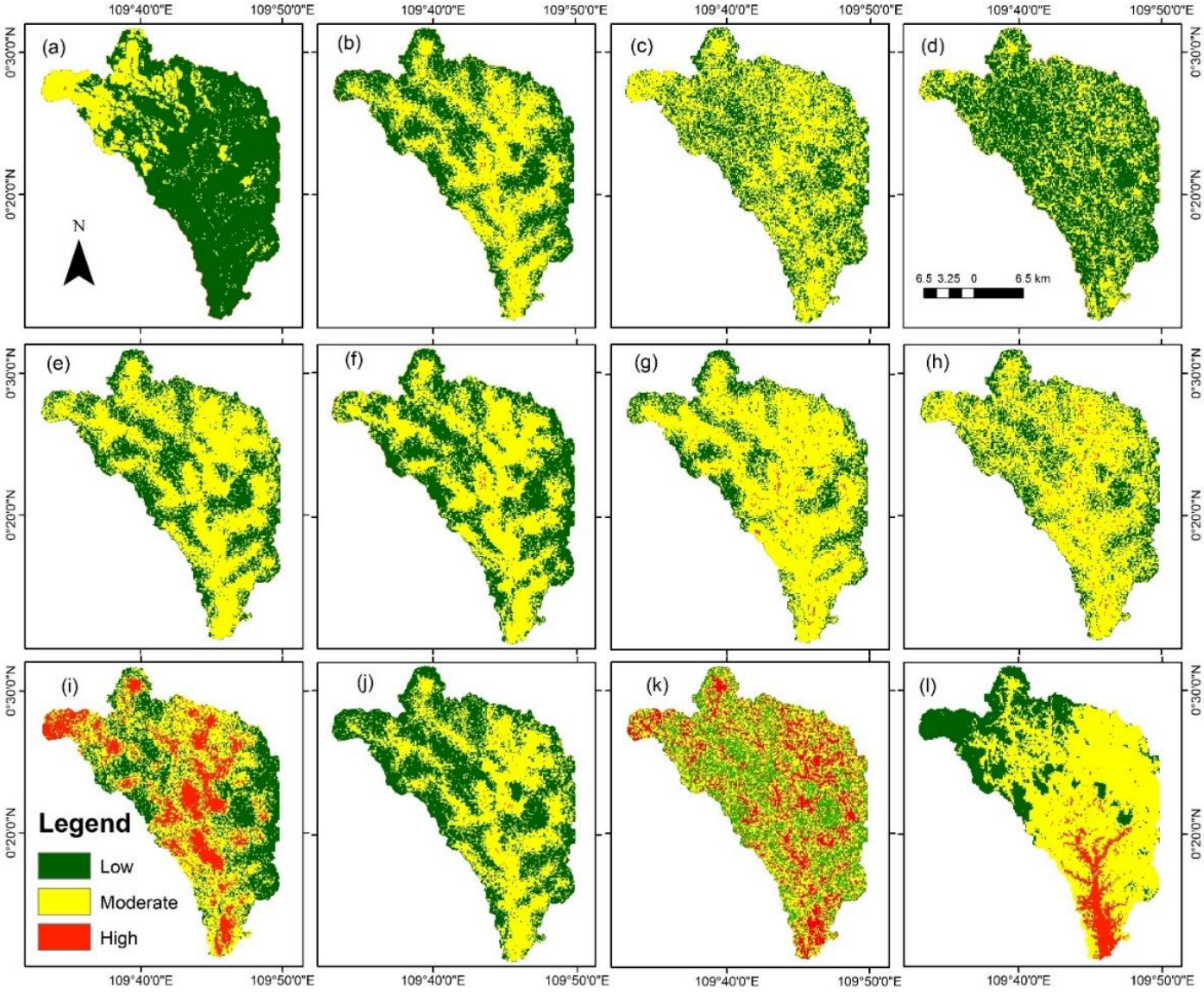

Figure 7. Comparison of several GIS-based and SAR-based Flood Susceptibility Maps, where from (a) to (k) present the scenario 1 to 11, respectively, and (l) is the SAR-based flood map.

The accuracy and dependability of flood models can be increased by recognizing the significance of these aspects and calculating the best weighting for each. Decisions about land use planning, development, and emergency response can all be made with the use of this information. It is important to keep in mind that not all places and situations may be suited to the weighting scenarios employed in the study. Other factors can range greatly from one region to another, and so can the best way to weight them. Consequently, additional study is required to improve and confirm these findings in various settings.

4. Conclusion

SAR data can be used to provide an optimum weighting scenario of GIS-based flood susceptibility maps. It also provides insights into complex factors contributing to flood susceptibility. Some of the advantages of this approach are its flexibility, ease of handling, and low cost, making it possible to apply it to areas where there is a lack of detailed information, when the aim is to obtain large-scale good risk maps, or when policymakers require a rapid flood risk assessment. This approach can fill a crucial gap in information by providing valid flood susceptibility maps to inform stakeholders and to enable communities to develop strategies such as levee construction or early warning systems to mitigate flood impacts. Flood susceptibility mapping has significant implications for advancing scientific understanding and managing flood risk to protect communities.

Acknowledgements

The authors would like to thank Land Rehabilitation, and Soil Conservation (Forestry Service) and Disaster Management Service West Kalimantan Province has provided the data and other research facilities.

Author Contributions

Conceptualization: Ajun Purwanto, Dony Andrasmoro, Eviliyanto Eviliyanto, Rustam Rustam, Mohd Hairy Ibrahim, Arif Rohman; **methodology**: Ajun Purwanto, Dony Andrasmoro, Eviliyanto Eviliyanto, Rustam Rustam, Mohd Hairy Ibrahim, Arif Rohman; **investigation**: Ajun Purwanto, Dony Andrasmoro, Eviliyanto Eviliyanto, Rustam Rustam, Mohd Hairy Ibrahim, Arif Rohman; **writing—original draft preparation**: Ajun Purwanto, Dony Andrasmoro, Eviliyanto Eviliyanto, Rustam Rustam; **writing—review and editing**: Ajun Purwanto, Dony Andrasmoro, Eviliyanto Eviliyanto, Rustam Rustam, Mohd Hairy Ibrahim, Arif Rohman; **visualization**: Mohd Hairy Ibrahim, Arif Rohman. All authors have read and agreed to the published version of the manuscript.

References

Adiat, K. A. N., Nawawi, M. N. M., & Abdullah, K. (2012). Assessing the accuracy of GIS-based elementary multi criteria decision analysis as a spatial prediction tool–a case of predicting potential zones of sustainable groundwater resources. Journal of Hydrology, 440, 75–89.

Alemayehu, Z. (2007). Modeling of Flood hazard management for forecasting and emergency response of 'Koka'area within Awash River basin using remote sensing and GIS method. Addis Ababa University.

Allafta, H., & Opp, C. (2021). GIS-based multi-criteria analysis for flood prone areas mapping in the trans-boundary Shatt Al-Arab basin, Iraq-Iran. Geomatics, Natural Hazards and Risk, 12(1), 2087–2116.

Anusha, N., & Bharathi, B. (2020). Flood detection and flood mapping using multi-temporal synthetic aperture radar and optical data. The Egyptian Journal of Remote Sensing and Space Science, 23(2), 207–219.

Biswajeet, P., & Mardiana, S. (2009). Flood hazrad assessment for cloud prone rainy areas in a typical tropical environment. Disaster Advances, 2(2), 7–15.

Blistanova, M., Zeleňáková, M., Blistan, P., & Ferencz, V. (2016). Assessment of flood vulnerability in Bodva river basin, Slovakia. Acta Montanistica Slovaca, 21(1).

Bubeck, P., Botzen, W. J. W., & Aerts, J. C. J. H. (2012). A review of risk perceptions and other factors that influence flood mitigation behavior. Risk Analysis: An International Journal, 32(9), 1481–1495.

Cai, S., Fan, J., & Yang, W. (2021). Flooding Risk Assessment and Analysis Based on GIS and the TFN-AHP Method: A Case Study of Chongqing, China. Atmosphere, 12(5), 623.

Chen, A. S., Evans, B., Djordjević, S., & Savić, D. A. (2012). Multi-layered coarse grid modelling in 2D urban flood simulations. Journal of Hydrology, 470, 1–11.

Clement, M. A., Kilsby, C. G., & Moore, P. (2018). Multi-temporal synthetic aperture radar flood mapping using change detection. Journal of Flood Risk Management, 11(2), 152–168.

Curebal, I., Efe, R., Ozdemir, H., Soykan, A., & Sönmez, S. (2016). GIS-based approach for flood analysis: Case study of Keçidere flash flood event (Turkey). Geocarto International, 31(4), 355–366.

Desalegn, H., & Mulu, A. (2021). Flood vulnerability assessment using GIS at Fetam watershed, upper Abbay basin, Ethiopia. Heliyon, 7(1), e05865.

Elkhrachy, I. (2015). Flash flood hazard mapping using satellite images and GIS tools: A case study of Najran City, Kingdom of Saudi Arabia (KSA). The Egyptian Journal of Remote Sensing and Space Science, 18(2), 261–278.

Falguni, M., & Singh, D. (2020). Detecting flood prone areas in Harris County: A GIS based analysis. GeoJournal, 85(3), 647–663.

Gazi, M. Y., Islam, M. A., & Hossain, S. (2019). Flood-hazard mapping in a regional scale way forward to the future hazard atlas in Bangladesh. Malaysian J. Geosci, 3(1), 1–11.

Geographic, N. (2019). Floods. Available online:https://www.nationalgeographic.com/environment/ natural-disasters/floods/.

Ghimire, B., Chen, A. S., Guidolin, M., Keedwell, E. C., Djordjević, S., & Savić, D. A. (2013). Formulation of a fast 2D urban pluvial flood model using a cellular automata approach. Journal of Hydroinformatics, 15(3), 676–686.

Gigović, L., Pamučar, D., Bajić, Z., & Drobnjak, S. (2017). Application of GIS-interval rough AHP methodology for flood hazard mapping in urban areas. Water, 9(6), 360.

Greene, R. G., & Cruise, J. F. (1995). Urban watershed modeling using geographic information system. Journal of Water Resources Planning and Management, 121(4), 318–325.

Hagen-Zanker, A. (2006). Comparing continuous valued raster data: A cross disciplinary literature scan [Monograph]. http://epubs.surrey.ac.uk/790371/

Hagos, Y. G., Andualem, T. G., Yibeltal, M., & Mengie, M. A. (2022). Flood hazard assessment and mapping using GIS integrated with multi-criteria decision analysis in upper Awash River basin, Ethiopia. Applied Water Science, 12(7), 1–18.

Haq, M., Akhtar, M., Muhammad, S., Paras, S., & Rahmatullah, J. (2012). Techniques of remote sensing and GIS for flood monitoring and damage assessment: A case study of Sindh province, Pakistan. The Egyptian Journal of Remote Sensing and Space Science, 15(2), 135–141.

Islam, M. M., & Sado, K. (2000). Development of flood hazard maps of Bangladesh using NOAA-AVHRR images with GIS. Hydrological Sciences Journal, 45(3), 337–355.

Jamali, B., Löwe, R., Bach, P. M., Urich, C., Arnbjerg-Nielsen, K., & Deletic, A. (2018). A rapid urban flood inundation and damage assessment model. Journal of Hydrology, 564, 1085–1098.

Komolafe, A. A., Awe, B. S., Olorunfemi, I. E., & Oguntunde, P. G. (2020). Modelling flood-prone area and vulnerability using integration of multi-criteria analysis and HAND model in the Ogun River Basin, Nigeria. Hydrological Sciences Journal, 65(10), 1766–1783.

Krzysztofowicz, R. (1993). A theory of flood warning systems. Water Resources Research, 29(12), 3981–3994. https://doi.org/10.1029/93WR00961

Li, Y., Martinis, S., Plank, S., & Ludwig, R. (2018). An automatic change detection approach for rapid flood mapping in Sentinel-1 SAR data. International Journal of Applied Earth Observation and Geoinformation, 73, 123–135. https://doi.org/10.1016/j.jag.2018.05.023

Mandal, S. P., & Chakrabarty, A. (2016). Flash flood risk assessment for upper Teesta River basin: Using the hydrological modeling system (HEC-HMS) software. Modeling Earth Systems and Environment, 2(2), 59.

Mason, D. C., Giustarini, L., Garcia-Pintado, J., & Cloke, H. L. (2014). Detection of flooded urban areas in high resolution Synthetic Aperture Radar images using double scattering. International Journal of Applied Earth Observation and Geoinformation, 28, 150–159.

Negese, A., Worku, D., Shitaye, A., & Getnet, H. (2022). Potential flood-prone area identification and mapping using GIS-based multi-criteria decision-making and analytical hierarchy process in Dega Damot district, northwestern Ethiopia. Applied Water Science, 12(12), 255. https://doi.org/10.1007/s13201-022-01772-7

Ozkan, S. P., & Tarhan, C. (2016). Detection of flood hazard in urban areas using GIS: Izmir case. Procedia Technology, 22, 373–381.

Paudyal, G. N. (1996). An integrated GIS-numerical modelling system for advanced flood management. Proceeding of the International Conference on Water Resources and Environment Research: Towards the 21st Century, Kyoto University, Japan, 555–562.

Petrucci, O. (2022). Factors leading to the occurrence of flood fatalities: a systematic review of research papers published between 2010 and 2020. Natural hazards and earth system sciences, 22(1), 71-83.

Post, P. (2021). Https://pontianakpost.jawapos.com/pontianakpost/15/01/2021/banjir-terjang-landak-25-desa-terendam-ribuan-warga-masih-bertahan-di-rumah.

Pradhan, B., Shafiee, M., & Pirasteh, S. (2009). Maximum flood prone area mapping using RADARSAT images and GIS: Kelantan River basin. International Journal of Geoinformatics, 5(2).

Rimba, A. B., Setiawati, M. D., Sambah, A. B., & Miura, F. (2017). Physical flood vulnerability mapping applying geospatial techniques in Okazaki City, Aichi Prefecture, Japan. Urban Science, 1(1), 7.

Rincón, D., Khan, U. T., & Armenakis, C. (2018). Flood risk mapping using GIS and multi-criteria analysis: A greater Toronto area case study. Geosciences, 8(8), 275.

Robinson, S. A., & Rai, V. (2015). Determinants of spatio-temporal patterns of energy technology adoption: An agent-based modeling approach. Applied Energy, 151, 273–284. https://doi.org/10.1016/j.apenergy.2015.04.071

Rohman A., Comber A. and Mitchell G. 2019 Evaluation of Natural Flood Management using Curve Number in the Ciliwung Basin, West Java. AGILE 2018 2-5

Romanescu, G., Hapciuc, O. E., Minea, I., & Iosub, M. (2018). Flood vulnerability assessment in the mountain–plateau transition zone: A case study of Marginea village (Romania). Journal of Flood Risk Management, 11, S502–S513.

Rozalis, S., Morin, E., Yair, Y., & Price, C. (2010). Flash flood prediction using an uncalibrated hydrological model and radar rainfall data in a Mediterranean watershed under changing hydrological conditions. Journal of Hydrology, 394(1–2), 245–255.

Sarmah, T., Das, S., Narendr, A., & Aithal, B. H. (2020). Assessing human vulnerability to urban flood hazard using the analytic hierarchy process and geographic information system. International Journal of Disaster Risk Reduction, 50, 101659.

Shafapour Tehrany, M., Shabani, F., Neamah Jebur, M., Hong, H., Chen, W., & Xie, X. (2017). GIS-based spatial prediction of flood prone areas using standalone frequency ratio, logistic regression, weight of evidence and their ensemble techniques. Geomatics, Natural Hazards and Risk, 8(2), 1538–1561.

Singh, A. P., Arya, A. K., & Singh, D. Sen. (2020). Morphometric analysis of Ghaghara River Basin, India, using SRTM data and GIS. Journal of the Geological Society of India, 95(2), 169–178.

Skilodimou, H. D., Bathrellos, G. D., Chousianitis, K., Youssef, A. M., & Pradhan, B. (2019). Multi-hazard assessment modeling via multi-criteria analysis and GIS: a case study. Environmental Earth Sciences, 78(2), 47.

Tay, C. W., Yun, S.-H., Chin, S. T., Bhardwaj, A., Jung, J., & Hill, E. M. (2020). Rapid flood and damage mapping using synthetic aperture radar in response to Typhoon Hagibis, Japan. Scientific Data, 7(1), 100.

UN SPIDER. (2019). Step-by-Step: Recommended Practice: Flood Mapping and Damage Assessment Using Sentinel-1 SAR Data in Google Earth Engine | UN-SPIDER Knowledge Portal. https://www.un-spider.org/advisory-support/recommended-practices/recommended-practice-google-earth-engine-flood-mapping/step-by-step

Visser, H., & Nijs, T. (2006). The Map Comparison Kit. Environmental Modelling & Software, 346–358. https://doi.org/10.1016/j.envsoft.2004.11.013

Vojtek, M., & Vojteková, J. (2019). Flood susceptibility mapping on a national scale in Slovakia using the analytical hierarchy process. Water, 11(2), 364.

Wondim, Y. K. (2016). Flood hazard and risk assessment using GIS and remote sensing in lower Awash sub-basin, Ethiopia. Journal of Environment and Earth Science, 6(9), 69–86.

Zhang, S., & Pan, B. (2014). An urban storm-inundation simulation method based on GIS. Journal of Hydrology, 517, 260–268.

Zhou, Q., Su, J., Arnbjerg-Nielsen, K., Ren, Y., Luo, J., Ye, Z., & Feng, J. (2021). A GIS-Based Hydrological Modeling Approach for Rapid Urban Flood Hazard Assessment. Water, 13(11), 1483.

Appendix 1. Python Script for GIS-based Weighted Overlay Automation

```
import arcpy
from arcpy.sa import *

arcpy.env.workspace = "E:/temila/new_result4/hasil4.gdb"

# Local variables:
slope_cls = "slope_cls"
precip = "precip"
drain_cls_ok = "drain_cls_ok"
soil = "soil"
lulc_cls = "lulc_cls"
altitude_ok2 = "altitude_ok2"
distance_to_river = "distance_to_river"
ndvi_cls = "ndvi_cls"
curve_cls_ok = "curve_cls_ok"
flowacc_cls = "flowacc_cls"
twi_class = "twi_class"
basinpilih = "basinpilih"
arcpy.env.extent = basinpilih
arcpy.env.mask = basinpilih

# Reading the scenarios table:
scenarios = arcpy.SearchCursor("scenario","","")

# Iterating the processes:
for row in scenarios:
    s_no = row.getValue("Factor")
    slope = float(row.getValue("Sl"))
    rain = float(row.getValue("Rf"))
    drain = float(row.getValue("DD"))
    soil_score = float(row.getValue("ST"))
    lulc = float(row.getValue("LULC"))
    elevation = float(row.getValue("El"))
    river = float(row.getValue("DR"))
    ndvi = float(row.getValue("NDVI"))
    curve = float(row.getValue("Ct"))
    flow_acc = float(row.getValue("FA"))
    twi = float(row.getValue("TWI"))
    print(s_no)

    rslt_ori = "rslt_"+str(s_no)
    rslt_ori_cls = "rslt_cls_"+str(s_no)
    RasterT_rslt_or1 = "rslt_poly_"+str(s_no)
    RasterT_rslt_or1_PolygonToRa = "rslt_res_"+str(s_no)
    flood__ASC = "E:\\temila\\new_result4\\asc6\\flood_"+str(s_no)+".ASC"

    result = (Raster(slope_cls)*slope) + (Raster(precip) *rain)+ (Raster(drain_cls_ok)
*drain)+(Raster(soil) *soil_score)+(Raster(lulc_cls) *lulc)+(Raster(altitude_ok2) *ele-
vation) +(Raster(distance_to_river) *river) +(Raster(ndvi_cls) *ndvi) +(Ras-
ter(curve_cls_ok) *curve) +(Raster(flowacc_cls) *flow_acc) +(Raster(twi_class) *twi)
    result.save(rslt_ori)

    # Process: Reclassify
    arcpy.gp.Reclassify_sa(rslt_ori, "Value", "1 2.33 1;2.34 3.67 2;3.68 5 3",
rslt_ori_cls,"DATA")

    # Process: Raster to Polygon
    arcpy.RasterToPolygon_conversion(rslt_ori_cls, RasterT_rslt_or1, "NO_SIMPLIFY",
"VALUE", "MULTIPLE_OUTER_PART", "")
```

```
    # Process: Polygon to Raster
    arcpy.PolygonToRaster_conversion(RasterT_rslt_or1, "GRIDCODE", Ras-
terT_rslt_or1_PolygonToRa, "CELL_CENTER", "NONE", "0.0011")

    # Process: Raster to ASCII
    arcpy.RasterToASCII_conversion(RasterT_rslt_or1_PolygonToRa, flood__ASC)
```